ARTICLES

Distribution of Vibrational States of CO_2 in the Reaction $O(^1D) + CO_2$ from Time-Resolved Fourier Transform Infrared Emission Spectra

Hui-Fen Chen

Department of Chemistry, National Tsing Hua University, Hsinchu 30013, Taiwan

Hung-Chu Chiang, Hiroyuki Matsui, and Soji Tsuchiya*

Department of Applied Chemistry and Institute of Molecular Science, National Chiao Tung University, Hsinchu 30010, Taiwan

Yuan-Pern Lee*

Department of Applied Chemistry and Institute of Molecular Science, National Chiao Tung University, Hsinchu 30010, Taiwan, and Institute of Atomic and Molecular Sciences, Academia Sinica, Taipei 10617, Taiwan

Received: August 21, 2008; Revised Manuscript Received: January 22, 2009

A mixture of O_3 and CO_2 was irradiated with light from a KrF laser at 248 nm; time-resolved infrared emission of CO_2 in the region 2000−2400 cm^{-1} was observed with a Fourier transform spectrometer. This emission involves one quantum in the asymmetric stretching mode (ν_3) of CO_2 in highly vibrationally excited states. The band contour agrees satisfactorily with a band shape calculated based on a simplified polyad model of CO_2 and a vibrational distribution estimated through a statistical partitioning of energy of ∼13 000 cm^{-1}, ∼3100 cm^{-1} smaller than the available energy, into the vibrational modes of CO_2. From this model, approximately 44% and 5% of the available energy of $O(^1D) + CO_2$ is converted into the vibrational and rotational energy of product CO_2, respectively, consistent with previous reports of ∼50% for the translational energy. An extent of rotational excitation of CO_2 much smaller than that expected from statistical calculations indicates a mechanism that causes a small torque to be given to CO_2 when an O atom leaves the complex CO_3 on the triplet exit surface of potential energy, consistent with quantum-chemical calculations.

Introduction

The excited electronic state of the oxygen atom $O(^1D_2)$ lies at 15 867 cm^{-1} above its ground state $O(^3P_2)$.[1] The reaction of $O(^1D_2)$ with CO_2 is of significant importance for several reasons. The quenching of $O(^1D)$ to $O(^3P)$ by small molecules is important, both experimentally and theoretically, because it involves the formation of a complex and likely a crossing of singlet and triplet surfaces; the transfer of electronic energy to vibration−rotational energy of these species in the stratosphere plays an important role in the atmospheric heat budget.[2,3] The reaction of $O(^1D)$ with CO_2 might involve exchange of O atoms. Understanding the corresponding isotopic exchange reactions is essential for the interpretation of the enrichment of ^{17}O and ^{18}O over ^{16}O of stratospheric CO_2 relative to tropospheric CO_2.[4−6] Spectral characterization of the stabilized reaction complex CO_3 is also important in extraterrestrial ices rich in carbon dioxide and in the atmospheres of Earth and Mars.[7−9]

Several isotope exchange experiments of $O(^1D) + CO_2$ have been reported.[10−14] On monitoring the rate of growth of $C^{16}O^{18}O$, Baulch and Breckenridge[13] investigated the exchange and quenching reactions of $O(^1D)$ with isotopic mixtures of $C^{16}O_2$ and $C^{18}O_2$, and suggested a nearly statistical scheme for isotopic exchange in which $O(^1D)$ reacting with CO_2 becomes incorporated into product CO_2 with an approximate probability of 2/3. Their finding is consistent with a formation of a long-lived CO_3 complex as a reaction intermediate. The lifetime of the CO_3 complex was estimated by DeMore and Dede[15] to be 1−10 ps based on their analysis of the observed decrease of quantum yield of O_3 upon UV irradiation of mixtures of O_3 and CO_2 under high pressure (100−2500 psi) at 243 K. The rate coefficient for quenching of $O(^1D)$ by CO_2 was reported by several groups to occur at nearly the rate of gas-kinetic collisions, on the order 10^{-10} cm^3 $molecule^{-1}$ s^{-1};[16−19] a small negative dependence of the rate coefficient on temperature was reported.[20] These facts are consistent with a quenching mechanism that involves an attractive surface of potential energy toward a long-lived complex CO_3.

Carbon trioxide CO_3 was identified in solid CO_2 and Ar matrix at low temperatures with IR absorption spectroscopy; the C_{2v} bridged structure was deduced to be more stable than the D_{3h} symmetric structure because only the former was observed.[9,10,21−23] A theoretical calculation of the system $O(^1D) + CO_2$ supported this result.[24] Calculations at various levels indicated that the energy difference between these two structures of CO_3 is within 1 kJ mol^{-1}, with a barrier of ∼18 kJ mol^{-1} from the most stable C_{2v} structure for interconversion.[9,25,26]

* To whom correspondence should be addressed. E-mail: yplee@mail.nctu.edu.tw (Y.-P.L.); sojitsuchiya@mail.nctu.edu.tw (S.T.).

10.1021/jp807501c CCC: $40.75
Published on Web 03/19/2009

To derive the nascent translational energies of O atoms, Matsumi et al.[27] measured the Doppler profiles of $O(^3P_J)$, with $J = 0, 1, 2$, as a function of delay between pump and probe laser pulses. $O(^1D)$ was produced on photolysis of N_2O at 193 nm, and $O(^3P_J)$ was observed with VUV laser-induced fluorescence. A fraction of 0.51 ± 0.03 of the available energy was released into relative translational motion between $O(^3P_J)$ and CO_2, indicating extensive internal excitation of CO_2. These authors suggested that the product channels $O(^3P_J) + CO_2$ are adiabatic, based on a nearly statistical distribution observed for the spin−orbit J states. Perri et al.[5,6] applied a crossed molecular beam to investigate the reaction $^{18}O(^1D) + C^{16}O_2$ and identified two collision channels forming $^{16}O(^3P) + C^{18}O^{16}O$ and $^{16}O(^1D) + C^{18}O^{16}O$, both via a CO_3 complex with a lifetime greater than its rotational period, with branching ratios of 0.84 and 0.67 at collision energies of 4.2 and 7.7 kcal mol^{-1}, respectively; the average translation energy amounts to ∼50% of the available energy, in agreement with the previous report of Matsumi et al.[27] Perri et al. indicated that, for a lifetime of the CO_3 complex sufficient to attain complete intramolecular vibrational relaxation (IVR), respective oxygen atoms of the complex should have an equal probability of ejection from the complex. If IVR in the complex were incomplete, the probability of ejecting the incoming oxygen atom or the other O atoms of CO_2 might be unequal, consequently causing an isotopic fractionation. The formation of a CO_3 complex was supported by Mebel et al., who employed multireference configuration interaction calculations to characterize the potential energy and applied statistical theories to derive rate coefficients of various channels including the intersystem singlet−triplet interactions.[26] Yang et al. proposed that quenching of $O(^1D)$ by CO_2 occurs through a complex CO_3 as well as a direct collision process.[25]

Here we present observations of the time-resolved IR emission spectra of product CO_2 from the quenching reaction of $O(^1D)$ by CO_2. We found satisfactory agreement between observed emission spectra of CO_2 and those simulated based on a vibrational distribution of CO_2 predicted with a statistical theory. In contrast, the average rotational energy is much smaller than that for a statistical distribution.

Experiments

The apparatus employed to obtain step-scan time-resolved Fourier transform spectra (TR-FTS) has been described previously;[28−30] only a summary is given here. A telescope mildly focused the photolysis beam from a KrF laser (248 nm, 23 Hz, ∼50 mJ) to an area $\sim 9 \times 10$ mm^2 at the reaction center to yield a fluence of ∼50 mJ cm^{-2}. The transient signal from an InSb detector with a rise time of 0.7 μs was preamplified with a gain factor of 10^5 V A^{-1} (EG&G Judson, PA9-50, 1.5 MHz bandwidth), followed by further amplification with a factor of 100 (bandwidth 1 MHz) before being digitized with an internal data-acquisition board (16 bit) at 5-μs resolution. Data were typically averaged over 60 laser pulses at each scan step; 1271 scan steps were performed to yield an interferogram resulting in a spectrum of resolution 4.0 cm^{-1} for CO_2 detection. The temporal response function of the instrument was determined with a pulsed IR laser beam, as described previously.[31] The spectral response function was calibrated using a blackbody radiation source.

Ozone (O_3) and CO_2 were injected separately into the reaction chamber. To decrease the collisional quenching of CO_2, a minimal pressure yielding acceptable signals was used: $P_{O_3} = 0.055-0.060$ Torr, $P_{CO_2} = 0.055-0.060$ Torr, and $P_{Ar} = 0-2.0$ Torr. Flow rates were $F_{O_3} = 1.9-2.1$ sccm, $F_{CO_2} = 1.9-2.1$ sccm, and $F_{Ar} = 0-69.6$ sccm; sccm denotes 1 cm^3 per min under standard conditions (273.15 K and 760 Torr). Most O_3 (∼60%) was dissociated upon irradiation at 248 nm based on the reported absorption cross section of 1.5×10^{-17} cm^2 molecule^{-1} for O_3 at 248 nm.[32] The depletion of O_3 in the flowing system after each laser pulse was modest, as was confirmed by the negligible variation of the signal when we decreased the repetition rate of the photolysis laser from 30 to 20 Hz.

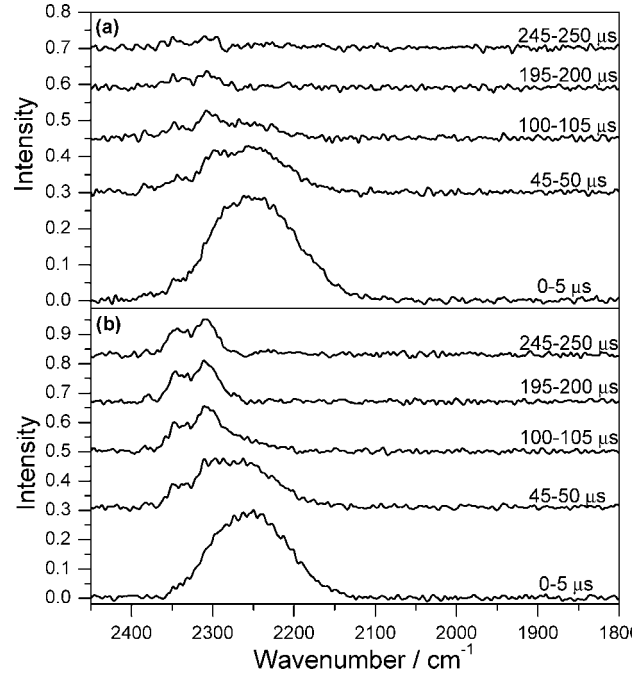

Figure 1. IR emission spectra from a mixture of O_3 and CO_2 at various periods after irradiation with light from a KrF excimer laser. Spectral resolution = 4 cm^{-1}. (a) $P_{O_3} = 0.060$ Torr and $P_{CO_2} = 0.060$ Torr. (b) $P_{O_3} = 0.055$ Torr, $P_{CO_2} = 0.055$ Torr, and $P_{Ar} = 1.754$ Torr.

CO_2 (AGA Specialty Gases, ≥99.99%) was used without purification except for degassing at 77 K. O_3 was produced from O_2 (Scott Specialty Gases, 99.995%) with an ozone generator (Polymetrics, Model T-408), stored over silica gel at 196 K. The partial pressure of O_3 was determined from the absorption of Hg emission at 254 nm in a cell of length 7.0 cm; the cross section for absorption of O_3 at 254 nm was taken to be 1.15×10^{-17} cm^2.[33]

Results and Discussion

A. Time-Resolved Fourier Transform Emission Spectra. Figure 1a shows emission spectra in a region of 2000−2450 cm^{-1} observed upon irradiation of mixture of O_3 (0.060 Torr) and CO_2 (0.060 Torr) with light at 248 nm from a KrF excimer laser. Only one broad emission band peak at about 2260 cm^{-1} with a full width at half-maximum (fwhm) of 125 cm^{-1} was observed for the period 0−5 μs. When Ar at a pressure of about 1.754 Torr was added to the system, a similar broad band was observed in the period 0−5 μs, with the peak position near 2260 cm^{-1} and fwhm 110 cm^{-1}, as shown in Figure 1b. At later periods, this feature shifted toward larger wavenumbers with its fwhm decreasing continuously; for the period 195−200 μs, the feature showed clearly the P- and R-branch structures with the band center increased to 2327 cm^{-1} and the fwhm decreased to 60 cm^{-1}.

We assign this feature to the ν_3 band of CO_2; at an early stage after photolysis of O_3, the band maximum is shifted to a smaller

wavenumber by about 90 cm^{-1} relative to the band center of the transition (0, 0^0, 1) → (0, 0^0, 0) at 2349.1 cm^{-1}. This shift is attributed to emission from highly internally excited CO_2 with anharmonic coupling between the (ν_1, ν_2) modes and the ν_3 mode, as is explained in detail in the next section. The vibrationally excited CO_2 is produced in the energy-transfer reaction

$$O(^1D) + CO_2 \rightarrow O(^3P) + CO_2^{\dagger} \quad (1)$$

for which the rate coefficient is about 1.1×10^{-10} cm^3 $molecule^{-1}$ s^{-1}.[16−20] Thus, under our experimental conditions, the band intensity rises to a maximum within 10 μs after the laser irradiation, and the emitting molecule suffers no deactivating collision within a few microseconds under a pressure less than 100 mTorr.

The shift in peak position of CO_2 emission at the later period is attributed to the vibration−vibration (V−V) energy transfer such as

$$CO_2(v_1, v_2^l, v_3) + CO_2(0, 0^0, 0) \rightarrow CO_2(v_1, v_2^l, v_3 - 1) + CO_2(0, 0^0, 1) \quad (2)$$

of which the rate coefficient would be large for nearly resonant conditions. The shape of (v_1, v_2^l, v_3) → (v_1, v_2^l, v_3 −1) bands of CO_2 near the region (0, 0^0, 1) → (0, 0^0, 0) is expected to be deformed due to strong self-absorption by CO_2 in its ground state.

The addition of Ar buffer gas at a pressure about 1.75 Torr is expected to thermalize rapidly the rotational distribution of CO_2, as shown in Figure 1b, but still maintaining nearly its nascent vibrational distribution. The observed band centers are approximately the same for the two spectra recorded with and without Ar, whereas the fwhm of 110 cm^{-1} for the feature in Figure 1b is smaller than the value of 125 cm^{-1} for the feature in Figure 1a, due to mainly rotational quenching. The rotational excitation of CO_2 for reaction 1 is hence relatively insignificant, and was readily thermalized by the added Ar buffer gas, to be discussed in detail in section E.

As for the vibrational relaxation at later intervals, the data in Figure 1b show more clearly the effect of the V−V energy transfer. The emission band at the delay of 195−200 μs is assigned to consist of mainly transitions of (v_1, v_2^l, 2) → (v_1, v_2^l, 1) and (v_1, v_2^l, 1) → (v_1, v_2^l, 0), in which the latter band is strongly self-absorbed. For a period greater than 100 μs, the feature in Figure 1b shows an intensity greater than that in Figure 1a, presumably because the emitting CO_2 diffuses from the detection area, in which the emission was collected with Welsh mirrors, more rapidly under low pressure.

B. Reaction Mechanism of $O(^1D) + CO_2$. The reader might refer to Figure 1 of ref 26 for various intermediates and transition states of the CO_3 system. According to high-level multireference quantum-chemical calculations by Mebel et al.,[26] the reactants first form a weakly bound complex (stabilized by ∼27.6 kJ mol^{-1}), which then rearranges via a barrier of ∼33 kJ mol^{-1} to C_{2v}-symmetric three-member cyclic CO_3, whose stabilization energy is 204 kJ mol^{-1} relative to $O(^1D) + CO_2$. The C_{2v}-symmetric CO_3 may further isomerize to the D_{3h}-symmetric CO_3 via a barrier of ∼18 kJ mol^{-1}; both isomers of CO_3 have similar energies. In the triplet electronic state, separated $O(^3P)$ and CO_2 have the lowest energies and they combine with each other through a transition state with barrier height ∼142 kJ mol^{-1} to form the triplet ($^3B_2$) CO_3 of a C_{2v} form which has an energy of ∼94 kJ mol^{-1} above the singlet CO_3 and ∼96 kJ mol^{-1} above that of $O(^3P) + CO_2$. A minimal energy crossing point (MSX) between the lowest triplet and singlet electronic surfaces is located near the triplet transition state; both the geometry and energy of MSX are similar to those of the triplet transition state. According to the calculations of rate coefficients of various channels, Mebel et al. indicated that formation of $O(^3P) + CO_2$ is mainly from the triplet CO_3 via the spin−orbit coupled radiationless transitions; only a small fraction (2−6%) of the $O(^3P) + CO_2$ products are produced directly from singlet CO_3 via the MSX. Hence, it is expected that singlet CO_3 is formed initially, followed by direct redissociation to $O(^1D) + CO_2$ or by the spin−orbit coupling to form triplet CO_3 before further dissociation to form $O(^3P) + CO_2$. Under our experimental conditions, the kinetic energy of $O(^1D)$ is not enough to populate CO_2 in its ν_3 state; hence no ν_3 emission of CO_2 from the singlet channel is expected to be observed in our experiments. The vibrationally excited CO_2 that we observed in this work is produced from dissociation of CO_3 on the triplet surface. According to previous experiments, CO_3 has a lifetime long enough for IVR and molecular rotation.[5,6,15] The available energy is likely partitioned statistically among the degrees of freedom for products $O(^3P)$ and CO_2 if the IVR is rapid, as indicated by previous experiments.

C. Approximate Level Energies of CO_2 Vibration. The energies of vibrationally excited CO_2 are defined as a function of quantum numbers v_1, v_2, and v_3 and l with the Dunham equation:

$$\begin{aligned} G(v_1, v_2^l, v_3) = {} & \omega_1 v_1 + \omega_2 v_2 + \omega_3 v_3 + x_{11} v_1^2 + \\ & x_{22} v_2^2 + x_{33} v_3^2 + x_{12} v_1 v_2 + x_{13} v_1 v_3 + x_{23} v_2 v_3 + x_{ll} l^2 + \\ & y_{111} v_1^3 + y_{112} v_1^2 v_2 + y_{113} v_1^2 v_3 + y_{122} v_1 v_2^2 + \\ & y_{123} v_1 v_2 v_3 + y_{133} v_1 v_3^2 + y_{222} v_2^3 + y_{223} v_2^2 v_3 + \\ & y_{233} v_2 v_3^2 + y_{333} v_3^3 + y_{1ll} v_1 l^2 + y_{2ll} v_2 l^2 + y_{3ll} v_3 l^2 \end{aligned} \quad (3)$$

in which $G(0, 0^0, 0)$ denotes the zero-point energy; we adopted values of the coefficients determined by Chedin.[34] As $\omega_1 \cong 2\omega_2$, the levels that satisfy a relation $2v_1 + v_2 =$ constant and having a common v_3 quantum number are nearly resonant; the levels of which quantum numbers in respective modes differ by $\Delta v_1 = \pm 1$, $\Delta v_2 = \mp 2$, and $\Delta v_3 = 0$ hence interact strongly with each other by Fermi couplings and form a polyad that is characterized with quantum number v_b as

$$v_b = 2v_1 + v_2 \quad (4)$$

Because the observed emission spectra of CO_2 show a broad feature and spectral parameters for highly vibrationally excited CO_2 are lacking, it is difficult to discuss in detail the level structure. We thus introduce an approximation in which one set of polyad levels is represented by a level (v_b, v_3) with an approximate degeneracy that is defined as the total number of levels within a polyad. For example, the polyad states with $v_b = 3$ and $v_3 = 0$ are composed of three *ungerade* states (1, 1^1, 0), (0, 3^1, 0), and (0, 3^3, 0) with a degeneracy of 6. Table 1 summarizes the parity and the degeneracy, $g(v_b)$, of the polyads having the quantum number v_b.

To define the representative level energy for the (v_b, v_3) polyad, we introduce average quantum numbers of v_1 and v_2, $\bar{v}_1$ and $\bar{v}_2$, taking into account the degeneracy for respective levels belonging to the polyad state as follows:

TABLE 1: Parity and Degeneracy of a Polyad of Vibrationally Excited CO_2

v_b	v_3	parity	degeneracy, $g(v_b)$
even	even	gerade	$\left(\frac{v_b+2}{2}\right)^2$
even	odd	ungerade	
odd	even	ungerade	$\left(\frac{v_b+1}{2}\right)\left(\frac{v_b+3}{2}\right)$
odd	odd	gerade	

$$\bar{v}_1 = \frac{v_b - \bar{v}_2}{2}, \qquad \bar{v}_2 = \frac{\sum_{1\text{ or }0}^{v_2} v_2 g'(v_b, v_2)}{\sum_{1\text{ or }0}^{v_2} g'(v_b, v_2)} \tag{5}$$

and

$$\bar{l} = \frac{\bar{v}_2}{2} \quad \text{for } \bar{v}_2 = \text{even}, \qquad \bar{l} = \frac{\bar{v}_2 + 1}{2} \quad \text{for } \bar{v}_2 = \text{odd} \tag{6}$$

in which the degeneracy for respective levels, $g'(v_b, v_2)$, equals $v_2 + 1$; the representative energy level is thereby calculated.

D. Statistical Partitioning of Available Energy. As mentioned previously, the quenching reaction of $O(^1D_2)$ with CO_2 proceeds through a long-lived intermediate CO_3; the electronic energy of $O(^1D_2)$ is likely partitioned statistically among the degrees of freedom for products $O(^3P_J)$ and CO_2.

Thelen et al. observed the velocity distribution of $O_2(^1\Delta)$ produced from photodissociation of O_3 with the 248 nm excimer laser light and determined the average space-fixed kinetic energy of $O(^1D)$ to be 36 kJ mol^{-1}, which is equivalent to 3009 cm^{-1}.[35] The distribution is over a wide energy range up to 72 kJ mol^{-1} because $O_2(^1\Delta)$ is vibrationally excited with $v = 0-5$. The relaxation of translational energy of $O(^1D)$ is fast. Assuming that the relaxation rate coefficients are the same for O_2, O_3, and CO_2 and using $k_E = 1.53 \times 10^{-10}$ cm^3 molecule^{-1} s^{-1} (in O_2) determined by Matsumi et al.,[36] we estimate the upper limit of average kinetic energy of $O(^1D)$ at 5 μs after photolysis to be $E_t = 16.6$ kJ mol^{-1}, corresponding to 1388 cm^{-1}. In the center-of-mass coordinates, the kinetic energy of the system, including the equilibrium thermal energy of 82 cm^{-1} for translation energy of CO_2 at room temperature, becomes 13.2 kJ mol^{-1} (1103 cm^{-1}). As the distribution of spin−orbit states of $O(^3P_J)$ is assumed to be statistical, the average energy of $O(^3P_J)$ is 77 cm^{-1}. This maximal available energy E^* for the reaction $O(^1D) + CO_2$, 15 868 + 1130 − 77 = 16 894 cm^{-1}, is partitioned among the relative translation energy E_t between products $O(^3P)$ and CO_2 and the internal energy of CO_2, i.e.

$$E^* = E_t + E_r + E_v \tag{7}$$

in which E_r and E_v are rotational and vibrational energies of CO_2, respectively. With CO_2 and O_3 used in our experiments, the quenching of $O(^1D)$ is expected to be faster, though corresponding rate coefficients are lacking; hence the kinetic energy in the center-of-mass system is expected to be smaller than 1103 cm^{-1}. If the kinetic energy of $O(^1D)$ is thermalized rapidly, the available energy would be 15 868 + 310 − 77 = 16 101 cm^{-1}, in which 310 cm^{-1} is the thermal translational energy between O and CO_2 at room temperature.

To obtain the statistical distribution of vibrational energy of CO_2, we calculate the density of respective vibrational states. This density for rotational and vibrational states with energies E_r and E_v, respectively, is formulated as[37]

$$N(E_r, E_v) = (2J + 1)\, g(E_v)\, C_t (E^* - E_r - E_v)^{1/2} \tag{8}$$

in which $2J + 1$ and $g(E_v)$ are the degeneracies of rotational and vibrational states, respectively, and $C_t(E^* - E_r - E_v)^{1/2}$, in which $C_t = 2\pi(2\mu/h^2)^{3/2}$, is the state density for translation. If we sum $N(E_r, E_v)$ over all possible rotational states, the density of vibrational states is derived as

$$N(E_v) = \sum_J^{J_{max}} N(E_v, E_r) = \int_0^{J_{max}} (2J + 1)\, g(E_v)\, C_t (E^* - E_v - E_r)^{1/2}\, dJ \tag{9}$$

Taking into account that $d[J(J + 1)] = (2J + 1)\, dJ$ and $E_r = BJ(J + 1)$, the density of states at vibrational state E_v becomes

$$N(E_v) = \left(\frac{2}{3B}\right) g(E_v)\, C_t (E^* - E_v)^{3/2} \tag{10}$$

The vibrational distribution probability $p^\circ(E_v)$ is calculated from the density of states with the equation

$$p^\circ(E_v) = \frac{N(E_v)}{\sum_v^{v_{max}} N(E_v)} \tag{11}$$

The distributions in respective (v_b, v_3) states shown in Figure 2 with $E^* = 16\,100$ cm^{-1} (see section E) indicate that much of the electronic energy of $O(^1D)$ is converted into vibrational energy of CO_2 in its symmetric stretching (ν_1) and bending (ν_2) modes rather than in the antisymmetric stretching (ν_3) mode because of the large degeneracy of the bending polyad states.

E. Simulation of Emission Spectra of CO_2. The emission observed in the region 2100−2400 cm^{-1} is assigned to transitions involving a single quantum of CO_2 in ν_3 mode, $(v_1, v_2^l, v_3) \rightarrow (v_1, v_2^l, v_3 - 1)$. It should be noted that, although only emission involving $\Delta v_3 = -1$ was observed, these transitions involve $(v_1, v_2, v_3) \rightarrow (v_1, v_2, v_3 - 1)$ which contain the population information on the excited CO_2 in all vibrational modes, including the symmetric stretching and bending vibrations. In our approximation, this transition is treated as the transition $(v_b, v_3) \rightarrow (v_b, v_3 - 1)$, of which the wavenumber of the transition is formulated according to the Dunham expansion

$$\omega(v_b, v_3 \rightarrow v_b, v_3 - 1) = \omega_3 + x_{33}(2v_3 - 1) + x_{13}\bar{v}_1 + x_{23}\bar{v}_2 + y_{333}(3v_3^2 - 3v_3 + 1) + y_{113}\bar{v}_1^2 + y_{223}\bar{v}_2^2 + (y_{133}\bar{v}_1 + y_{233}\bar{v}_2)(2v_3 - 1) + y_{3ll}l^2 \tag{12}$$

in which $\bar{v}_1$ and $\bar{v}_2$ are the average quantum numbers defined in eq 5. To confirm the above approximation to be acceptable, we compared the wavenumbers of band origins for $v_b = 5$ [ref

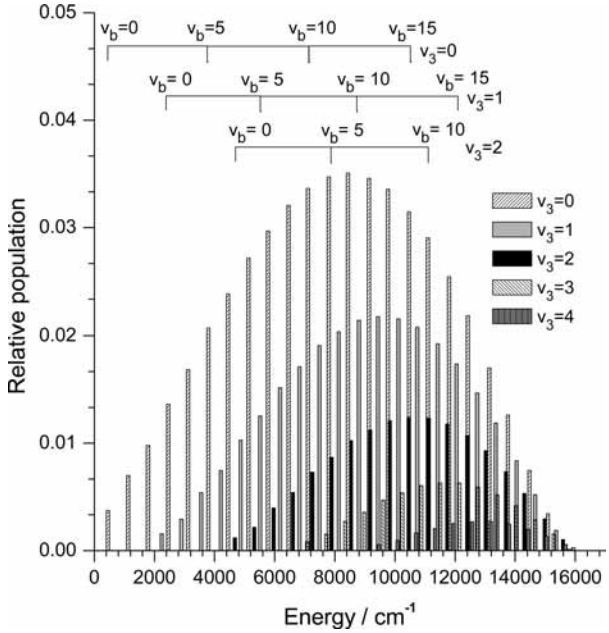

Figure 2. Statistical vibrational distribution of CO_2 (v_b, v_3) produced from $O(^1D) + CO_2$. Representative quantum numbers v_b are indicated for each v_3 series. The available energy used is 16 100 cm^{-1}; see text.

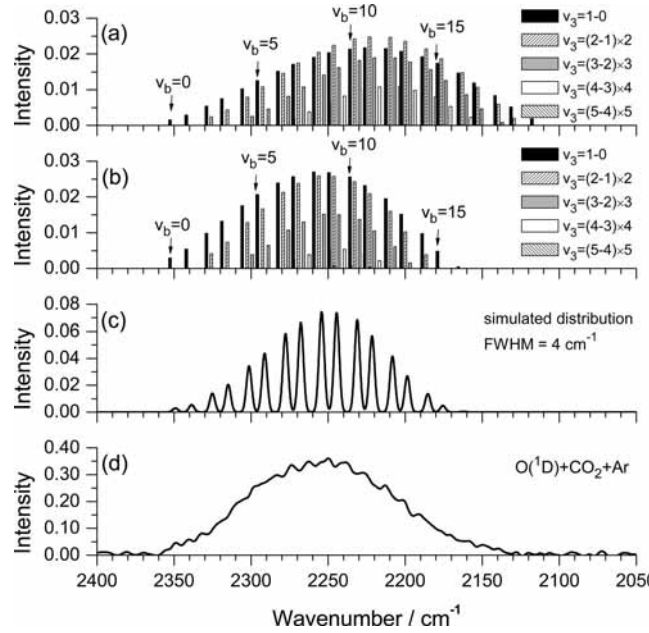

Figure 3. Comparison of observed emission spectrum of v_3 band of CO_2 with calculated band origins of v_3 transitions of CO_2 of which the vibrational levels are shown in Figure 2. (a) Calculated band origins of transitions (v_b, v_3) → (v_b, $v_3 - 1$); representative quantum numbers v_b are indicated for each $v_3 \rightarrow v_3 - 1$ series using $E^* = 16\,100$ cm^{-1}. (b) Same as (a) except $E^* = 13\,000$ cm^{-1}. (c) Simulated vibrational intensity distribution contour using Gaussian with fwhm = 4 cm^{-1} for each component in (a). (d) Observed emission of CO_2 as in Figure 1b.

38] and 6 [ref 39] of CO_2 from the emission of a discharged mixture of $N_2 + CO_2$ with the values of the present approximation using $\bar{v}_1$ and $\bar{v}_2$; the agreement is within ±3.4 and ±4.5 cm^{-1} for $v_b = 5$ and 6, respectively.

Because observation of rotationally resolved lines is unlikely, we simulate the spectra by assuming a statistical distribution of vibrational levels with total energy E^*, as described in the previous section. The intensity of transition (v_b, v_3) → (v_b, $v_3 - 1$) of excited CO_2 is described as

$$I(v_b, v_3 \rightarrow v_3 - 1) \propto \omega(v_b, v_3 \rightarrow v_3 - 1) \, A(v_b, v_3 \rightarrow v_3 - 1)\, p^\circ(v_b, v_3) \quad (13)$$

in which $A(v_b, v_3 \rightarrow v_3 - 1)$ is the rate of radiative transition that is assumed to be independent of v_b and proportional to v_3. In Figure 3a, the relative emission intensities for respective vibrational transitions (v_b, $v_3 \rightarrow v_b$, $v_3 - 1$) based on the statistically partitioned vibrational distribution of CO_2 with E^* of 16 100 cm^{-1} are given as stick diagrams. This statistical partition shows poor agreement with the experimental observation, shown in Figure 3d, for the $O(^1D) + CO_2 + Ar$ experiment in which rotational distribution of CO_2 should be nearly thermalized; observed maximal distribution lies at wavenumbers much greater than the calculation. An improved fitting was derived by decreasing the E^* value to 13 000 cm^{-1}; calculated spectral distribution is shown in Figure 3b. To compare with the vibrational distribution of the observed spectrum shown in Figure 3d, we employed a Gaussian function of fwhm (full-width at half-maximum) = 4 cm^{-1} to integrate the intensities of each component in Figure 3b to yield Figure 3c. This is a simple comparison of vibrational distribution without consideration of rotational profiles.

For comparison of the contours of emission bands, we applied the program PGopher developed by Western[40] to simulate the rotational contours of CO_2 using rotational constants 0.390, 0.387, 0.384, 0.381, and 0.379 cm^{-1} for $v_3 = 1$, 2, 3, 4, and 5, respectively, and $J \leq 150$.[34] For this calculation we assumed that rotational contours for P and R branches on each side of the respective vibrational transitions to be identical for all v_b given in Figure 3b as an example. We varied E^* and the rotational temperature to obtain the best fit between the experimentally observed profile and the simulated one. In Figure 4a, the spectrum observed upon photolysis of a mixture of O_3 (0.060 Torr) and CO_2 (0.060 Torr) is compared with the spectra simulated with $E^* = 13\,000$ cm^{-1}. The thick line indicates the observed spectrum and the thin line indicates the simulated spectrum with the specified rotational temperature; the shaded areas represent the uncertainty limits ± 200 K. Figure 4a shows satisfactory agreement between experimental and simulated spectra; the error of fitting the available energy E^* is estimated to be ~500 cm^{-1}. The band shape is mainly determined by the available energy E^*; the rotational energy has only a limited effect on the band shape and has little effect on the position of the maximal intensity.

According to a statistical partitioning of $E^* = 13\,000$ cm^{-1} among three modes of CO_2, approximately 81% of available energy is distributed to the ν_1 and ν_2 modes and 19% to the ν_3 mode; the fraction of electronic energy of $O(^1D)$ converted to vibrational excitation of CO_2 is ~44% of the available energy (16 100 cm^{-1}) and ~54% of the fitted E^*. It should be noted that the average vibrational energy is derived from the observed band contour which determines the distribution of vibrational levels; hence it is insensitive to the fitted E^* value.

A rotational temperature of 1100 ± 200 K produces the best fit of the calculated envelope with the observed band profile, as shown in Figure 4a. This rotational temperature is equivalent to ~760 ± 150 cm^{-1}, which corresponds to 5 ± 1% of the available energy. Taking into account that 44% of available energy is channeled to vibrational excitation of CO_2, in total ~49% of the available energy is converted to internal energy of CO_2, consistent with the reported value of ~50% for the

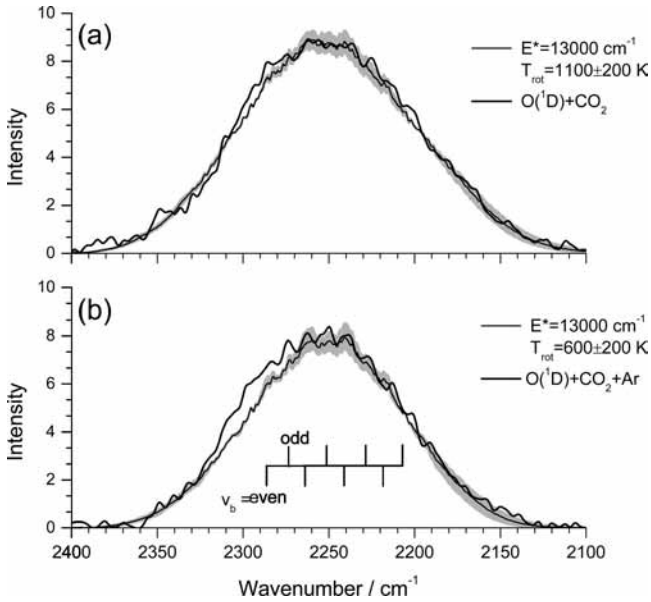

Figure 4. Comparison of calculated vibration−rotational band envelope with observed CO_2 emission band observed 0−5 μs after photolysis. (a) $P_{O_3} = 0.060$ Torr and $P_{CO_2} = 0.060$ Torr. Simulation with $E^* = 13\,000$ cm^{-1} and rotational temperature of 1100 ± 200 K. (b) $P_{O_3} = 0.055$ Torr, $P_{CO_2} = 0.055$ Torr, and $P_{Ar} = 1.754$ Torr; simulation with $E^* = 13\,000$ cm^{-1} and rotational temperature of 600 ± 200 K. Experimental data, thick line; simulated data, thin line with error limits represented by shaded area.

translational energy from measurements of the kinetic energy of product $O(^3P)$[27] or CO_2.[5,6]

Assuming statistical distribution and following eq 8, we express the density of states for rotation of CO_2 having average vibrational energy $\langle E_v \rangle$ as

$$N(E_r) = (2J + 1)\, g(\langle E_v \rangle)\, C_t (E^* - \langle E_v \rangle - E_r)^{1/2} \quad (14)$$

The average rotational energy of CO_2 is consequently given as

$$\langle E_r \rangle = \frac{\int_0^{E_r^{max}} E_r (E^* - \langle E_v \rangle - E_r)^{1/2}\, dE_r}{\int_0^{E_r^{max}} (E^* - \langle E_v \rangle - E_r)^{1/2}\, dE_r} = \frac{2}{5}(E^* - \langle E_v \rangle) \quad (15)$$

If we introduce 44% of available energy as $\langle E_v \rangle$, then $\langle E_r \rangle$ must be 23%. This efficiency of conversion of energy of $O(^1D)$ into rotation of product CO_2 is much larger than the value of ∼5% estimated from the observed band envelope. We thus conclude that the statistical partitioning of the $O(^1D)$ energy into rotational freedom is not realized. The present quenching reaction proceeds through the long-lived intermediate CO_3 which dissociates toward $O(^3P) + CO_2$ after crossing to the triplet surface. Partitioning of the reaction energy into rotation of the product molecule is induced by a torque between the separating product atom and molecule. According to a quantum-chemical calculation of the $O + CO_2$ reaction system,[26] the transition structure on the triplet surface has an elongated C−O bond of 1.52 Å and a CO_2 moiety having two C═O bonds with an angle of 146°. If the O atom leaves CO_2 along the C_2 axis of the transition structure toward the formation of $O(^3P) + CO_2$, the O atom might not exert a torque sufficient to excite the rotational motion of CO_2. Our observation of little rotational excitation of CO_2 is consistent with this scheme predicted with quantum-chemical calculations. In a similar quenching reaction of $O(^1D)$ with CO, the electronic energy of $O(^1D)$ is partitioned statistically to vibration of CO.[41] The fraction of the reaction energy disposed into vibration of CO is $f_v \cong 0.21$,[42] similar to the value of 0.24 from the prior distribution, whereas the fraction into rotation of CO is $f_r \cong 0.17$, smaller than the statistical value of 0.30 given by eq 15. It has been pointed out that the rotational distributions of the product molecules often deviate significantly from prior distributions even for the reactions that proceed over a fairly deep well.[37] For example, Kleinermanns et al.[43] reported that, in reactions involving long-lived intermediates such as $CO_2 + H$, $O_2 + H$, and $O(^1D) + H_2$, the energy disposal into rotation of the product OH is not statistical.

It is unclear why the fitted E^* is ∼3100 cm^{-1} smaller than the available energy of 16 100 cm^{-1}. Although we are using a simplified polyad model which uses anharmonicity terms determined only for levels up to ∼10 000 cm^{-1}, we think that possible associated errors cannot account for the difference between fitted E^* and the total available energy. The decomposition of CO_3 to form $O(^3P) + CO_2$ is on the triplet surface rather than the singlet surface. It is possible that some of the electronic excitation energy (∼7870 cm^{-1}) of CO_3 is unfeasible for equipartition into the vibrational distribution of CO_2; hence the fitted E^* is smaller than the maximal available energy. The reaction energy does not have to be equipartitioned into vibrational levels of the product molecule even when the reaction involves a long-lived complex.[37] The internal energy of the complex must be randomized, but the partitioning of available energy into internal and translational degrees of freedom is determined by reaction dynamics when the complex decomposes into products via a transition state. According to Mebel et al.,[26] the transition state on the triplet CO_3 surface has an elongated C−O bond of 1.52 Å and a CO_2 moiety having two C═O bonds with lengths ∼1.22 Å and an angle of 146°. When the elongated C−O bond is broken, extensive excitation of translational energy and bending vibrations of CO_2 is expected. An E^* value smaller than the available energy is not unusual. Further spectral information on the highly vibrationally excited states of CO_2 and more sophisticated reaction dynamic calculations on the singlet−triplet crossing are needed in order to decipher the difference between observed E^* and the total available energy.

Rotationally excited CO_2 is expected to attain thermal equilibrium rapidly when the Ar gas is present at pressure ∼ 2 Torr and 295 K. For the spectrum observed upon photolysis of a mixture of O_3 (0.055 Torr), CO_2 (0.055 Torr), and Ar (1.754 Torr), a spectrum simulated with a rotational contour corresponding to 600 ± 200 K fits satisfactorily the observed spectrum, as shown in Figure 4b; the thick line indicates the observed spectrum and the thin line indicates the simulated spectrum for $T = 600$ K with the shaded area representing the uncertainty limits ± 200 K. We noted that the spectrum observed when Ar was added, as presented in Figure 4b, showed distinct structures more enhanced than those observed when Ar was absent, as in Figure 4a, presumably due to rotational quenching. This structure showing intensity maxima with alternating spacings of ∼12 and 9 cm^{-1} is satisfactorily represented with our simulated spectrum. In our simulation, the spectrum shows spacings of ∼21 cm^{-1} for even-numbered v_b or odd-numbered v_b, corresponding well to the anharmonicity of x_{13}, −19.1 cm^{-1},[34] whereas the separations between the even-numbered v_b and their next member of (odd) v_b, ∼12 cm^{-1}, corresponds well with the anharmonicity of x_{23}, −12.5 cm^{-1}, as illustrated in Figure 4b. The agreement between the observed and the

simulated spectra indicates that the simple polyad model is adequate in describing the vibrational excitation of CO_2.

Conclusion

In the quenching of $O(^1D)$ by CO_2, we observed an emission band involving the ν_3 mode of highly vibrationally excited CO_2. The band contour agrees with a shape calculated based on the vibrational distribution estimated from a statistical partitioning of 13 000 cm^{-1}, ~3100 cm^{-1} smaller than the available energy, into the vibrational modes of CO_2. Approximately 44% of the available energy is converted to vibrational degrees of freedom of product CO_2. The rotational temperature of product CO_2 was estimated to be 1100 ± 200 K from the band contour; the extent of the rotational excitation of CO_2 thus corresponds to ~5% of available energy. The rotational excitation much smaller than that expected from a statistical calculation indicates a mechanism that associates with a small torque to be given to CO_2 when O atom is dissociated from the complex CO_3 on the triplet exit surface of potential energy, consistent with that predicted with quantum-chemical calculations.

Acknowledgment. The National Science Council of Taiwan supported this work under Contract No. NSC96-2113-M009-025. S.T. is grateful to the National Science Council of Taiwan for a Distinguished Visiting Professorship at National Chiao Tung University, Hsinchu, Taiwan.

References and Notes

(1) Wiese, W. L.; Fuhr, J. R.; Deters, T. M. *J. Phys. Chem. Ref. Data, Monogr.* **1996**, No. 7.
(2) Taylor, R. L. *Can. J. Chem.* **1974**, *52*, 1436.
(3) Harris, R. D.; Adams, G. W. *J. Geophys. Res.* **1983**, *88*, 4918.
(4) Lammerzahl, P.; Rockmann, T.; Brenninkmeijer, C. A. M.; Krankowsky, D.; Mauersberg, K. *Geophys. Res. Lett.* **2002**, *29*, 1582, and references therein.
(5) Perri, M. J.; Van Wyngarden, A. L.; Boering, K. A.; Lin, J. J.; Lee, Y. T. *J. Chem. Phys.* **2003**, *119*, 8213.
(6) Perri, M. J.; Van Wyngarden, A. L.; Lin, J. J.; Lee, Y. T.; Boering, K. A. *J. Phys. Chem. A* **2004**, *108*, 7995.
(7) Yung, Y. L.; DeMore, W. B. *Photochemistry of Planetary Atmospheres*; Oxford University Press: Oxford, U.K., 1999.
(8) Bogard, D. D.; Clayton, R. N.; Marti, K.; Owen, T.; Turner, G. *Space Sci. Rev.* **2001**, *96*, 425.
(9) Bennett, C. J.; Jamieson, C.; Mebel, A. M.; Kaiser, R. I. *Phys. Chem. Chem. Phys.* **2004**, *6*, 735.
(10) Katakis, D.; Taube, H. *J. Chem. Phys.* **1962**, *36*, 416.
(11) Yamazaki, H.; Cvetanović, R. J. *J. Chem. Phys.* **1964**, *40*, 582.
(12) Preson, K. F.; Cvetanović, R. J. *J. Chem. Phys.* **1966**, *45*, 2888.
(13) Baulch, D. L.; Breckenridge, W. H. *Trans. Faraday Soc.* **1966**, *62*, 2768.
(14) Weissberger, E.; Breckenridge, W. H.; Taube, H. *J. Chem. Phys.* **1967**, *47*, 1764.
(15) DeMore, W. B.; Dede, C. *J. Phys. Chem.* **1970**, *74*, 2621.
(16) Davidson, J. A.; Sadowski, C. M.; Schiff, H. I.; Streit, G. E.; Howard, C. J.; Jennings, D. A.; Schmeltekopf, A. L. *J. Chem. Phys.* **1976**, *64*, 57.
(17) Young, R. A.; Black, G.; Slanger, T. G. *J. Chem. Phys.* **1968**, *49*, 4758.
(18) Wine, P. H.; Ravishankara, A. R. *Chem. Phys. Lett.* **1981**, *77*, 103.
(19) Dunlea, E. J.; Ravishankara, A. R. *Phys. Chem. Chem. Phys.* **2004**, *6*, 2152.
(20) Streit, G. E.; Howard, C. J.; Schmeltekopf, A. L.; Davidson, J. A.; Schiff, H. I. *J. Chem. Phys.* **1976**, *65*, 4761.
(21) Moll, N. G.; Clutter, D. R.; Thompson, W. E. *J. Chem. Phys.* **1966**, *45*, 4469.
(22) Weissberger, E.; Breckenridge, W. H.; Taube, H. *J. Chem. Phys.* **1967**, *47*, 1764.
(23) Jacox, M. E.; Milligan, D. E. *J. Chem. Phys.* **1971**, *54*, 919.
(24) Froese, R. D. J.; Goddard, J. D. *J. Phys. Chem.* **1993**, *97*, 7484.
(25) Yang, G.; Yao, L.; Zhang, X.; Meng, Q.; Han, K.-L. *Int. J. Quantum Chem.* **2005**, *105*, 154.
(26) Mebel, A. M.; Hayashi, M.; Kislov, V. V.; Lin, S. H. *J. Phys. Chem. A* **2004**, *108*, 7983.
(27) Matsumi, Y.; Inagaki, Y.; Morley, G. P.; Kawasaki, M. *J. Chem. Phys.* **1994**, *100*, 315.
(28) Wu, C.-Y.; Chung, C.-Y.; Lee, Y.-C.; Lee, Y.-P. *J. Chem. Phys.* **2002**, *117*, 9785.
(29) Yeh, P.-S.; Leu, G.-H.; Lee, Y.-P.; Chen, I.-C. *J. Chem. Phys.* **1995**, *103*, 4879.
(30) Lin, S.-R.; Lee, Y.-P. *J. Chem. Phys.* **1999**, *111*, 9233.
(31) Yang, S.-K.; Liu, S.-Y.; Chen, H.-F.; Lee, Y.-P. *J. Chem. Phys.* **2005**, *123*, 224304.
(32) Matsumi, Y.; Kawasaki, M. *Chem. Rev.* **2003**, *103*, 4767.
(33) DeMore, W. B.; Raper, O. *J. Phys. Chem.* **1964**, *68*, 412.
(34) Chedin, A. *J. Mol. Spectrosc.* **1979**, *76*, 430.
(35) Thelen, M. A.; Gejo, T.; Harrison, J. A.; Huber, J. R. *J. Chem. Phys.* **1995**, *103*, 7946.
(36) Matsumi, Y.; Shamsuddin, S. M.; Sato, Y.; Kawasaki, M. *J. Chem. Phys.* **1994**, *101*, 9610.
(37) Levine, R. D.; Bernstein, R. B. *Molecular Reaction Dynamics and Chemical Reactivity*; Oxford University Press: New York, 1985.
(38) Bailly, D.; Tashkun, S. A.; Perevalov, V. I.; Teffo, J. L.; Arcas, P. H. *J. Mol. Spectrosc.* **1998**, *190*, 1.
(39) Bailly, D. *J. Mol. Spectrosc.* **1998**, *192*, 257.
(40) Western, C. M. *PGOPHER, a program for simulating for rotational structure*; http://pgopher.chm.bris.ac.uk.
(41) Shortridge, R. G.; Lin, M.-C. *J. Chem. Phys.* **1976**, *64*, 4076.
(42) Chen, H.-F.; Lee, Y.-P. *J. Phys Chem. A* **2006**, *110*, 12096.
(43) Kleinermanns, K.; Linnebach, E.; Wolfrum, J. *J. Phys. Chem.* **1985**, *89*, 2525.

JP807501C